Transportation Research Part C 85 (2017) 429–450

Contents lists available at ScienceDirect

Transportation Research Part C

journal homepage: www.elsevier.com/locate/trc

Variable speed limit design based on mode dependent Cell Transmission Model☆

Alfréd Csikós[a,*], Balázs Kulcsár[b]

[a] Institute for Computer Science and Control, Hungarian Academy of Sciences, Budapest, Hungary
[b] Department of Electrical Engineering, Chalmers University of Technology, Gothenburg, Sweden

ARTICLE INFO

Keywords:
Motorway traffic control
Cell Transmission Model
PWA system
switching control
Variable speed limit control

ABSTRACT

In this paper a mode dependent variable speed limit (VSL) control strategy is developed for motorway networks. The suggested rolling horizon and coordinated algorithm uses switching mode Cell Transmission Model (CTM) and purports to maximize network throughput.

In this line, first, a VSL signal scheduled piecewise affine switching mode CTM is derived based on the polyhedral description of Godunov fluxes. Second, a two-stage, coordinated, rolling horizon VSL sequence generation procedure is proposed. The set of possible VSL signs is selected by applying input constraints in order to eliminate spatial and temporal VSL oscillations. Then, the set of modes is further reduced according to the *stable* and adjacent reachable modes of the switching mode CTM. Over the remaining set of input signals, network capacity is maximized with the help of solving a mixed integer optimization problem under the form of reference density tracking objective. The method is implemented in simulation environment to demonstrate its computational efficiency and viability to attenuate shockwaves.

1. Introduction

The continuously growing road transport demand may traditionally be addressed by expanding the available road infrastructure, i.e. road construction. This physical expansion of the network is not only costly or sometimes very challenging (e.g. in urban areas), but also may adapt to changing traffic conditions in a rather conservative way. Hence, Intelligent Transport Systems (ITS) have been applied as an alternative to track the dynamic demand patterns. In motorway networks, such efficiency (and safety) indicators try to compensate traffic congestion in order to decrease travel delay, emission, energy consumption and crash risk, etc.

In order to capture the macroscopic and dynamic traffic patterns on motorways, different traffic flow models have been proposed. A first order model, governed by the vehicle conservation law and including the fundamental relationship between flow and density was suggested by Lighthill and Whitham (1955) and Richards (1956). Based on the discretization scheme of Godunov (1959), a numerical solution is given to the LWR model resulting in the well-known Cell Transmission Model (CTM) by Daganzo (1994). CTM is convenient in terms of describing capacity changes since it is capable of interpreting kinematic (congestion and rarefaction) waves.

Assuming a triangular form for the fundamental diagram, the model can be reformulated as switching mode dynamics belonging to the class of piecewise affine model representations, see Sontag (1981). This form is very attractive for model-based traffic management (traffic state estimation and control), for two main reasons: (i) scalability and computational burden (ii) it is control theory supported, Borrelli et al. (2011).

☆ This article belongs to the Virtual Special Issue on “Future Traffic Management”.

* Corresponding author.
E-mail address: csikos.alfred@sztaki.mta.hu (A. Csikós).

http://dx.doi.org/10.1016/j.trc.2017.10.003
Received 28 October 2016; Received in revised form 18 August 2017; Accepted 3 October 2017
Available online 16 October 2017
0968-090X/

With this switching concept in mind network state estimation problem has been considered in Kurzhanskiy (2009), Canudas De Wit et al. (2012), Morbidi et al. (2014), Vivas et al. (2015), and Sun and Work (2014) via modes associated to each cell by distinguished Godunov flux pairs. An effective solution to mode-related traffic state estimation is proposed by means of wavefront localization: in case of N segments, $N + 1$ operation modes are defined, see Munoz et al. (2003) and Morarescu and Canudas De Wit (2011). A joint estimation-ramp control problem is proposed in Sun et al. (2003). The approach defines two main controller modes: all-congested and all-free-flow cell conditions. In Thai and Bayen, 2013, 2015 an explicit piecewise affine decomposition of the Godunov scheme is formulated for network state estimation of uncontrolled systems, leading to a polyhedral description of operation modes. This approach provides a complete description of the system modes, for the entire state domain of each cell.

Motorway control measures - i.e. ramp metering and variable speed limit (VSL) control - need special modelling efforts when applying to the CTM. Mode dependent CTM has been formalized for (mostly local) ramp metering but only a few studies deal with speed limit control solutions. In the works Jacquet et al. (2006) and Lemarchand et al. (2011), robust ramp meter design approaches are suggested. Similarly to the previous works, the number of switching modes are determined with the help of jamwave front localization. Furthermore, the appropriate restriction of boundary conditions can lead to efficient switching mode based ramp solution, see Gomes et al. (2008). Focusing on the ramp metering problem, control-oriented switching mode representations are given in Pisarski and de Wit (2012) and Ferrara et al. (2015). In both cases, the operation modes are selected including the effect of ramp metering over the traffic flow conditions resulting in a rule-based control solution.

Variable speed limit control has only been considered in a limited number of papers with CTM. With mode dependent CTM, Muralidharan and Horowitz (2015) divides the coordinated ramp metering-VSL problem to several subproblems, according to the flow conditions at the cell interfaces. Each problem is then relaxed and solved as an effective linear programming problem. An online model predictive control (MPC) approach for VSL inclusion is presented in Hadiuzzaman and Tony (2013). In that work no switching mode description is used, instead, CTM is treated as a nonlinear model due to the minimum conditions of Godunov flows. A thorough discussion of speed limit modeling with the triangular fundamental diagram is given by Han et al. (2017). The proposed VSL model is applied for CTM, and the minimum conditions of the CTM are used to define a relaxed linear problem in Han et al. (2017).

Using the shockwave theory, the method SPECIALIST by Hegyi et al. (2008) proposes an easily implementable time-update free, feedforward control solution for coordinated VSL. Our proposed controller scheme uses similar concept, however, a recursive VSL is considered via the dynamics of CTM.

The aim of the present paper is to develop a systematic methodology for motorway traffic flow control through a switching mode CTM-based VSL design algorithm. In this line, our contribution is twofold. First, as an extension of the works by Thai and Bayen (2013, 2015), the inclusion of VSL into the framework of polyhedral CTM description is shown. In the derived form the system matrices as well as the polyhedral representation of the system are triggered by the control signal, i.e. an (input) parameter-dependent PWA model is obtained. Second, a coordinated VSL control algorithm is proposed. After reducing the set of input signals by means of spatial and temporal constraints (similarly as in Frejo et al. (2014)), an analysis of reachable modes is carried out and those signals are kept that provide reachability of stable modes for the highest number of segments. Over the remaining set of control signals an optimization is carried out to maximize network throughput on a finite prediction horizon.

With the current technique developed we intend to show that an appropriate handling of the VSL included CTM enables a very effective control for shockwave suppression. During control design, the input dependence of the polyhedral representation of the system is exploited. Numerical results affirm that the analysis of reachable modes during control set reduction has a key role in obtaining a controller with a fast response and low computational demand.

The layout of the paper is as follows. In Section 2, the CTM is reviewed alongside its polyhedral representation, summarizing the modelling contributions of Thai and Bayen (2013, 2015). Then, following the modelling assumptions, the polyhedral representation of the CTM is given for VSL controlled networks in Section 3. Control design is detailed in Section 4. Simulation results are shown in Section 5.

2. Preliminaries

2.1. The continuous LWR model

Lighthill and Whitham (1955) and Richards (1956) introduced a macroscopic dynamic model of traffic based on the conservation of vehicles:

$$\frac{\partial \rho(x,t)}{\partial t} + \frac{\partial q(x,t)}{\partial x} = r(x,t) - s(x,t), \tag{1}$$

where $\rho(x,t)$ and $q(x,t)$ denote the density and the flow of vehicles at location x and time t, respectively. Additional sources and sinks of traffic are represented by $r(x,t)$ and $s(x,t)$. In practice, these flows come from on- and off-ramps. The model adopts the hypothesis of Greenshields (1935), assuming a static flow-density relationship, known as the flow function:

$$q(x,t) = Q(\rho(x,t)). \tag{2}$$

Several flow functions have been suggested. The commonly used triangular flow function (see Fig. 1a) is given in the form

$$Q(\rho) = \begin{cases} v_f \rho & \text{if } \rho \leqslant \rho_{cr} \\ -w(\rho - \rho_{jam}) & \text{if } \rho > \rho_{cr} \end{cases}, \tag{3}$$

where ρ_{cr} and ρ_{jam} denote the critical and maximal traffic density respectively, and w denotes the backward propagating wave speed.

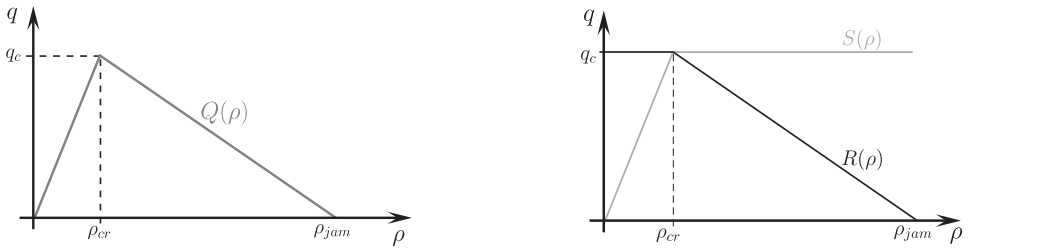

(a) Triangular flow function (b) Sending ($S(\rho)$) and receiving ($R(\rho)$) functions

Fig. 1. Triangular flow function represented in the LWR model and in the CTM.

2.2. Cell Transmission Model

Specifying $\rho(x,0)$ initial and $\rho(0,t)$ boundary conditions for Eq. (1), an initial value problem can be stated. Its analytic solution is obtained following the method of characteristics. In the engineering sense, characteristics represent moving perturbations of homogeneous density. Since the flow function is concave, both positive and negative characteristics can be present. In practice, this means that perturbations can propagate both upstream and downstream compared within the Eulerian coordinate frame. Therefore, to address moving perturbations in both directions, during the numeric solution of the initial value problem, the effect of the upstream and downstream information needs to be incorporated into the dynamics. This is satisfied by the discretization scheme of Godunov (1959). The application of the Godunov scheme for the continuous LWR model is known as the Cell Transmission Model (CTM), introduced by Daganzo (1994).

In the following, the Godunov discretization scheme is applied on Eq. (1), supposing that no sinks and sources are present. Spatial discretization is realized by an increment of length L_i whereas T denotes the temporal step.[1] The discrete space and time steps are indexed by i and k, respectively. According to the Godunov scheme, the law of conservation is obtained as follows:

$$\rho_i(k+1) = \rho_i(k) - \frac{T}{L_i}(G(\rho_i(k),\rho_{i+1}(k)) - G(\rho_{i-1}(k),\rho_i(k))), \tag{4}$$

where $G(\cdot,\cdot)$ denotes the Godunov flux, the realized flow between two neighbouring segments per lane. It can be expressed as the minimum of two intercellular fluxes - the sending flow $S(\rho)$ from the upstream segment i and the receiving flow $R(\rho)$ of the downstream segment $i+1$:

$$G(\rho_i,\rho_{i+1}) = \min(S(\rho_i),R(\rho_{i+1})). \tag{5}$$

The fluxes $S(\rho)$ and $R(\rho)$ can be defined by an appropriate partitioning of the flow function $Q(\rho)$ (as shown in Fig. 1b). The sending function describes the supply of traffic flow from an upstream segment, while the receiving function represents the absorption potential of a downstream segment. Formally:

$$S(\rho) = \begin{cases} v_f\rho & \text{if } \rho \leqslant \rho_{cr} \\ q_c & \text{if } \rho > \rho_{cr} \end{cases} \quad R(\rho) = \begin{cases} q_c & \text{if } \rho \leqslant \rho_{cr} \\ -w(\rho-\rho_{jam}) & \text{if } \rho > \rho_{cr}. \end{cases} \tag{6}$$

Using this scheme, the upstream segment supplies the flow through the boundary up to the capacity of the downstream segment. When the downstream segment is congested, its demand limits the flow through the boundary.

2.3. Polyhedral representation of the Godunov flux and switching description of dynamics

In this section an explicit polyhedral representation of the Godunov scheme is given, summarizing the results of Thai and Bayen (2013, 2015). The description provides a bivariate function for the Godunov flux over the space (ρ_i,ρ_{i+1}).

Assuming a triangular fundamental diagram, a piecewise affine function for the Godunov flux is given by

$$G(\rho_i,\rho_{i+1}) = \begin{cases} R(\rho_{i+1}) = -w(\rho_{i+1}-\rho_{jam}) & \text{if } (\rho_i,\rho_{i+1}) \in \mathrm{W} \\ q_c & \text{if } (\rho_i,\rho_{i+1}) \in \mathrm{L} \\ S(\rho_i) = v_f\rho_i & \text{if } (\rho_i,\rho_{i+1}) \in \mathrm{D}. \end{cases} \tag{7}$$

The space (ρ_i,ρ_{i+1}) then can be divided to the regions W, L and D (see Fig. 2) according to the rules

$$\mathrm{W} = \{(\rho_i,\rho_{i+1}):\ \rho_{i+1} > \rho_{cr}, \rho_{i+1} > h(\rho_i)\}, \tag{8}$$

$$\mathrm{L} = \{(\rho_i,\rho_{i+1}):\ \rho_i > \rho_{cr}, \rho_{i+1} \leqslant \rho_{cr}\}, \tag{9}$$

$$\mathrm{D} = \{(\rho_i,\rho_{i+1}):\ \rho_i \leqslant \rho_{cr}, \rho_{i+1} \leqslant h(\rho_i)\}. \tag{10}$$

[1] According to the CFL (Courant-Friedrich-Lewy) condition, the numeric solution of a hyperbolic PDE remains stable if the following statement is satisfied: $c_{max}\frac{T}{L_i} < 1$ where c_{max} denotes the maximal characteristic speed Courant et al. (1928).

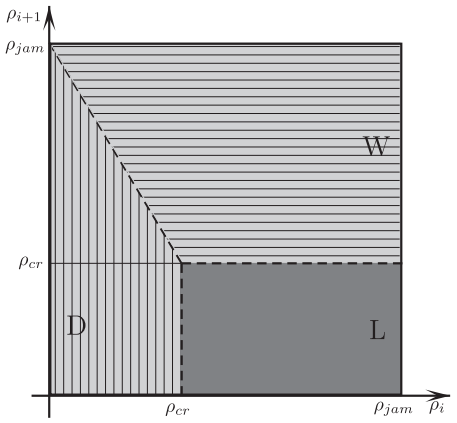

Fig. 2. Partition of the space (ρ_i,ρ_{i+1}).

Between regions W and D the boundary is given by the line

$$(\rho_i,\rho_{i+1}) = (\rho_i,h(\rho_i)), \quad \rho_i < \rho_{cr}, \tag{11}$$

with the function h defined as

$$h(\rho_i) = R^{-1}(S(\rho_i)) = -\frac{v_f}{w}\rho_i + \rho_{jam}. \tag{12}$$

Thus, a polyhedral partition of the space (ρ_i,ρ_{i+1}) is formulated and the corresponding $G(\rho_i,\rho_{i+1})$ flux function can be stated.

The dynamics of ρ_i depends on ρ_{i-1}, ρ_i and ρ_{i+1} through the fluxes $G(\rho_{i-1},\rho_i)$ and $G(\rho_i,\rho_{i+1})$. By substituting the polyhedral piecewise affine function of $G(\cdot,\cdot)$ from Eq. (7) to the conservation equation (4), a mode dependent description of Godunov scheme can be obtained. For segment i, state dynamics is given as

$$\rho_i(k+1) = J_{m_i}\begin{bmatrix}\rho_{i-1}(k)\\ \rho_i(k)\\ \rho_{i+1}(k)\end{bmatrix} + K_{m_i}, \tag{13}$$

where m_i denotes the mode of segment i. Eq. (13) is a switching mode dynamics for the CTM. Since three state regions are defined for each flux, a total of 9 modes may be defined for each segment. Excluding the non-feasible flux pairs,[2] 7 operation modes remain, listed in Table 1.

Table 1
Coefficient parameters of operation modes for a single segment.

m_i	(ρ_{i-1},ρ_i)	(ρ_i,ρ_{i+1})	J_{m_i}	K_{m_i}
1	W	W	$\left[0 \quad 1-\frac{T}{L_i}w \quad \frac{T}{L_i}w\right]$	0
2	W	L	$\left[0 \quad 1-\frac{T}{L_i}w \quad 0\right]$	$-\frac{T}{L_i}(v_f\rho_{cr}-w\rho_{jam})$
3	L	W	$\left[0 \quad 1 \quad \frac{T}{L_i}w\right]$	$-\frac{T}{L_i}(w\rho_{jam}-v_f\rho_{cr})$
4	L	D	$\left[0 \quad 1-\frac{T}{L_i}v_f \quad 0\right]$	$\frac{T}{L_i}v_f\rho_{cr}$
5	D	W	$\left[\frac{T}{L_i}v_f \quad 1 \quad \frac{T}{L_i}w\right]$	$-\frac{T}{L_i}w\rho_{jam}$
6	D	L	$\left[\frac{T}{L_i}v_f \quad 1 \quad 0\right]$	$-\frac{T}{L_i}v_f\rho_{cr}$
7	D	D	$\left[\frac{T}{L_i}v_f \quad 1-\frac{T}{L_i}v_f \quad 0\right]$	0

[2] according to the definitions of (8)–(10), contradiction of domains is present in flux pairs LL and WD, given by the condition ($\rho_i \leqslant \rho_{cr}$ and $\rho_i > \rho_{cr}$).

3. Polyhedral representation of CTM in case of VSL control

3.1. Assumptions and notations

Consider a network of N_s segments with no on- or off-ramps as depicted in Fig. 3.[3] According to this assumption, the state vector of the system contains the segment densities: $x(k) = [\rho_1,...,\rho_{N_s}]^T$. The boundary conditions of the system are considered as measured disturbances, collected in the vector $d(k) = [\rho_0(k)\,\rho_{N_s+1}(k)]^T$. The system is controlled by variable speed limit signals at each segment, concatenated in the vector $u(k) = [vsl_1(k),...,vsl_{N_s}(k)]^T$. In the boundary segments no control (i.e. $vsl_0 = vsl_{N_s+1} = v_f$) is active. Then, system dynamics is searched in the form

$$x(k+1) = f_{m(k)}(x(k),d(k),u(k)), \tag{14}$$

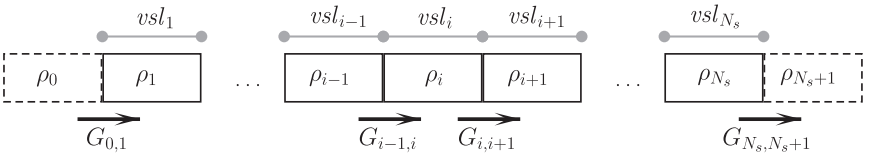

Fig. 3. Network layout.

where $m(k) = [m_1(k),...,m_{N_s}(k)]^T$ denotes the mode vector of the system.

The effect of variable speed limits is described through its effect on the sending and receiving functions (see Fig. 4). There is no change in parameters w and ρ_{jam}. Instead of v_f, the value of speed limit vsl_i is substituted, leading to a linear dependence in capacity reduction.[4] The modified free speed parameter entails the change in ρ_{cr} and q_c as follows

$$\rho_{cr}(vsl_i) = \frac{\rho_{jam} w}{w + vsl_i}, \tag{15}$$

$$q_c(vsl_i) = \rho_{cr}(vsl_i) vsl_i. \tag{16}$$

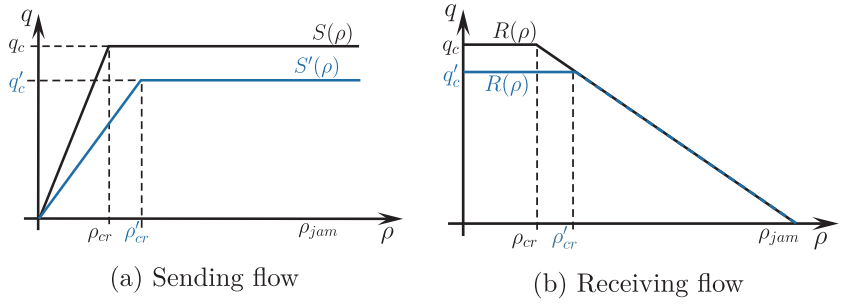

Fig. 4. Modifying effect of VSL control on sending and receiving flow functions.

Remark 1. Note, that in case of VSL activation, due to driver's behaviour, the parameter vsl_i in the actual operating fundamental diagram may not necessarily change exactly to the commanded speed limit signal. This effect is modelled by multiplying the commanded speed limit values by a constant α factor of the speed limit. Hence,

$$vsl_i = \alpha \cdot v_i^{ctrl} \tag{17}$$

is supposed, v_i^{ctrl} denoting the commanded signal. Without the loss of generality and for the sake of a concise model description, in the remaining of the paper, $\alpha = 1$ is considered.

3.2. Polyhedral description of the Godunov flux

The change in the sending and receiving functions necessitates the reformalization of the polyhedral representation of the Godunov flux function. Attention needs to be paid to the following points:

[3] Current work focuses on main lane capacity control. The presence of on-ramps means an additional possibility to control traffic demands of the network. Nevertheless, there exist motorway stretches along which no ramps or no controlled ramps are present and the control possibilities of the system are restricted.

[4] This assumption meets the approach of the works Papageorgiou et al. (2008), Hegyi et al. (2003), and Hadiuzzaman and Tony (2013). Note, however, that at low speed limits, capacity modifying effect of speed limits is reduced, Soriguera et al. (2017).

1. The partition of the space (ρ_i,ρ_{i+1}) is changed.
2. The value of the Godunov flux function also changes. Note that by definition (see Eq. (5)), it is the minimum of the functions $R(\rho_{i+1})$ and $S(\rho_i)$. The VSL affected sending and receiving fluxes are illustrated in Fig. 5.

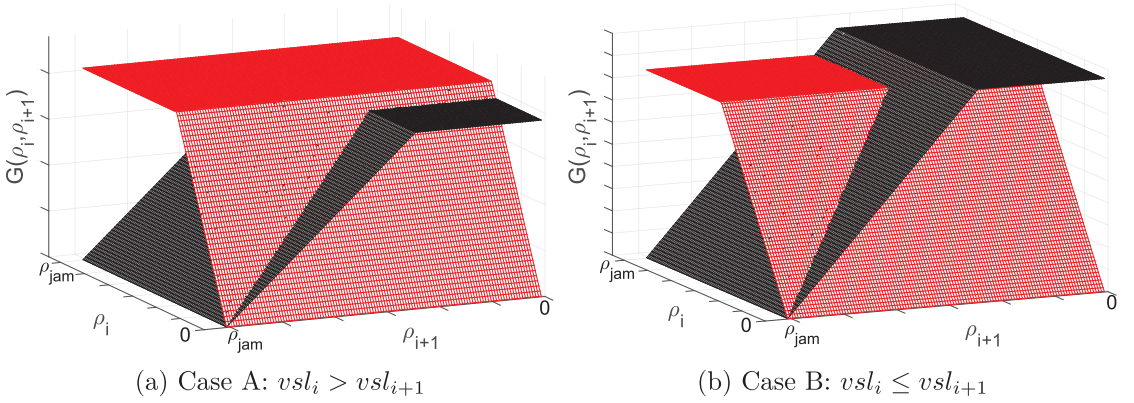

(a) Case A: $vsl_i > vsl_{i+1}$ (b) Case B: $vsl_i \leq vsl_{i+1}$

Fig. 5. Godunov fluxes in case of VSL control (red: $S(\rho_i)$, black: $R(\rho_{i+1})$). (For interpretation of the references to color in this figure legend, the reader is referred to the web version of this article.)

For both points, the relation between the upstream and downstream speed limit needs to be analysed. Two cases can be distinguished. In case A, $vsl_i > vsl_{i+1}$ (see Fig. 5a), while in case B, $vsl_i \leqslant vsl_{i+1}$ (see Fig. 5b). The general formalization of the two cases is stated after their separate derivation.

First, the VSL dependent formalization of the partition of (ρ_i,ρ_{i+1}) is outlined.

The modified definition of region boundaries can be understood by examining the projection of Fig. 5a and b to (ρ_i,ρ_{i+1}), illustrated in Fig. 6a and b.

In both cases, the regions are encased in the quadrants

W=□$_{ABEF}$
L=□$_{BCDE}$
D=□$_{ABCG}$.

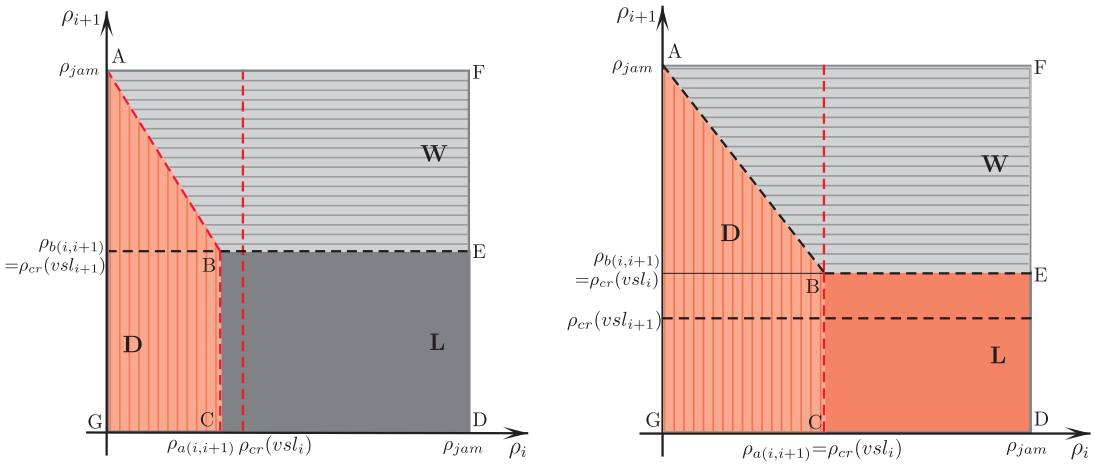

(a) Case A: $vsl_i > vsl_{i+1}$ (b) Case B: $vsl_i \leq vsl_{i+1}$

Fig. 6. Polyhedral representations of Godunov fluxes in case of VSL control.

The coordinates of the points B, C and E are given by vsl_i and vsl_{i+1} through $\rho_{a(i,i+1)}$ and $\rho_{b(i,i+1)}$. Their definitions can be given according to the relation between the speed limits.

- Case (A) $vsl_i > vsl_{i+1}$

$$\rho_{a(i,i+1)} = \frac{\rho_{cr}(vsl_{i+1})vsl_{i+1}}{vsl_i} \tag{18}$$

$$\rho_{b(i,i+1)} = \rho_{cr}(vsl_{i+1}). \tag{19}$$

- Case (B) $vsl_i \leqslant vsl_{i+1}$

$$\rho_{a(i,i+1)} = \rho_{cr}(vsl_i) \tag{20}$$

$$\rho_{b(i,i+1)} = \rho_{cr}(vsl_i). \tag{21}$$

By means of ρ_a and ρ_b region boundaries can be redefined as:

$$\begin{aligned}
&\mathrm{W}=\{(\rho_i,\rho_{i+1}):\ \rho_{i+1} > \rho_{b(i,i+1)},\rho_{i+1} > h(\rho_i)\}\\
&\mathrm{L}=\{(\rho_i,\rho_{i+1}):\ \rho_i > \rho_{a(i,i+1)},\rho_{i+1} \leqslant \rho_{b(i,i+1)}\}\\
&\mathrm{D}=\{(\rho_i,\rho_{i+1}):\ \rho_i \leqslant \rho_{a(i,i+1)},\rho_{i+1} \leqslant h(\rho_i)\}.
\end{aligned}$$

Regions W and D are separated by the line

$$h(\rho_i) = R^{-1}(S(\rho_i)) = -\frac{\rho_{jam}-\rho_{b(i,i+1)}}{\rho_{a(i,i+1)}}\rho_i + \rho_{jam}.$$

Note that the parameters $\rho_{a(i,i+1)}$ and $\rho_{b(i,i+1)}$ are only interpreted as region boundaries during the specification of Godunov flux modes. As a corollary, when analysing any three subsequent sections (indexed as $i-1$, i, $i+1$), for the middle section i, both $\rho_{a(i,i+1)}$ and $\rho_{b(i-1,i)}$ can be defined. Their relation, however, influences the number of feasible operation modes.

Proposition 1. *For the triplet ($i-1$, i, $i+1$), the relation $\rho_{a(i,i+1)} \leqslant \rho_{b(i-1,i)}$ always holds, regardless the relations among vsl_{i-1}, vsl_i, vsl_{i+1}.*

Proof. See Appendix A. □

As a consequence, dynamic mode of string pair 'WD' may not exist. However, in certain cases, 'LL' may exist.
In case of VSL control, the modified Godunov flux can be stated as a function of speed limits. Formally:

$$G(\rho_i,\rho_{i+1}) = \begin{cases} R(\rho_{i+1}) = -w(\rho_{i+1}-\rho_{jam}) & if\ (\rho_i,\rho_{i+1})\in \mathrm{W} \\ vsl_i\rho_{a(i,i+1)} & if\ (\rho_i,\rho_{i+1})\in \mathrm{L} \\ S(\rho_i) = vsl_i\rho_i & if\ (\rho_i,\rho_{i+1})\in \mathrm{D}. \end{cases} \tag{22}$$

3.3. Switching state dynamics

As a corollary of Proposition 1, an additional flux pair 'LL' can be defined. This leads to an additional 8th mode of the switching dynamics, see Table 2.

For segment ρ_i in mode m_i, state dynamics can be given by

Table 2
Coefficient parameters of operation modes for a single segment in case of VSL control.

m_i	(ρ_{i-1},ρ_i)	(ρ_i,ρ_{i+1})	$J_{m_i}(vsl_{i-1},vsl_i,vsl_{i+1})$	$K_{m_i}(vsl_{i-1},vsl_i,vsl_{i+1})$
1	W	W	$\begin{bmatrix} 0 & 1-\frac{T}{L_i}w & \frac{T}{L_i}w \end{bmatrix}$	0
2	W	L	$\begin{bmatrix} 0 & 1-\frac{T}{L_i}w & 0 \end{bmatrix}$	$-\frac{T}{L_i}(vsl_i\rho_{a(i,i+1)}-w\rho_{jam})$
3	L	W	$\begin{bmatrix} 0 & 1 & \frac{T}{L_i}w \end{bmatrix}$	$-\frac{T}{L_i}(w\rho_{jam}-vsl_{i-1}\rho_{a,(i-1,i)})$
4	L	D	$\begin{bmatrix} 0 & 1-\frac{T}{L_i}vsl_i & 0 \end{bmatrix}$	$\frac{T}{L_i}vsl_{i-1}\rho_{a,(i-1,i)}$
5	D	W	$\begin{bmatrix} \frac{T}{L_i}vsl_{i-1} & 1 & \frac{T}{L_i}w \end{bmatrix}$	$-\frac{T}{L_i}w\rho_{jam}$
6	D	L	$\begin{bmatrix} \frac{T}{L_i}vsl_{i-1} & 1 & 0 \end{bmatrix}$	$-\frac{T}{L_i}vsl_i\rho_{a,(i,i+1)}$
7	D	D	$\begin{bmatrix} \frac{T}{L_i}vsl_{i-1} & 1-\frac{T}{L_i}vsl_i & 0 \end{bmatrix}$	0
8	L	L	$[0 \quad 0 \quad 0]$	$\frac{T}{L_i}(vsl_{i-1}\rho_{a,(i-1,i)}-vsl_i\rho_{a,(i,i+1)})$

$$\rho_i(k+1) = J_{m_i}(vsl_{i-1}(k), vsl_i(k), vsl_{i+1}(k)) \begin{bmatrix} \rho_{i-1}(k) \\ \rho_i(k) \\ \rho_{i+1}(k) \end{bmatrix} + K_{m_i}(vsl_{i-1}(k), vsl_i(k), vsl_{i+1}(k)). \tag{23}$$

Proposition 2. *The VSL controlled network of N_s segments can be described by a parameter dependent Piecewise Affine model as PWA(u) in the form*

$$x(k+1) = A_1^m(u(k))\rho(k) + A_0^m(u(k)) + H_1^m(u(k))d(k), \tag{24}$$

where m denotes the mode vector of the system, $m = [m_1,...,m_{N_s}]^T$, $m_i \in 1,...,8$, $\forall\, i = 1,...,N_s$.

Proof. For the assumed network topology, from the matrices J_{m_i} and K_{m_i}, matrices A_1, A_0, H_1 can be built as follows

$$A_1^m = \begin{bmatrix} J_{m_1} & 0 & ... & 0 \\ 0 & J_{m_2} & ... & 0 \\ ... & ... & \ddots & ... \\ 0 & ... & 0 & J_{m_{N_s}} \end{bmatrix} \quad A_0^m = \begin{bmatrix} K_{m_1} \\ ... \\ K_{m_{N_s}} \end{bmatrix} \quad H_1^m = \begin{bmatrix} J_{m_0} & 0 \\ 0 & 0 \\ ... & ... \\ 0 & 0 \\ 0 & J_{m_{N_s+1}}, \end{bmatrix}.$$

Since the coefficients in Table 2 are stated as functions of the speed limits, an input-dependent affine form is obtained. □

3.4. Half-space representation of system modes

In the sequel, the half-space representation of the polyhedral system is investigated. This description provides a basis for the analysis of single-step adjacent system modes, which is a key step during the control design.

The domain of mode $m_i(k)$ for segment i is determined by the upstream and downstream flux modes of the segment

$$\mathrm{Dom}(m_i) = Q_{i-1,i} \bigcap Q_{i,i+1}, \tag{25}$$

where $Q_{i-1,i} \in \{W_{i-1,i}, L_{i-1,i}, D_{i-1,i}\}$. The eight modes of a single segment are depicted in Fig. 7.

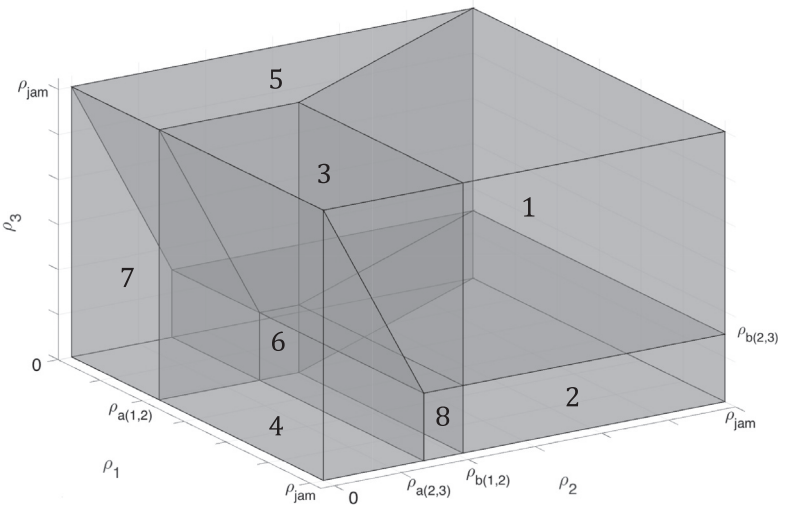

Fig. 7. Operation modes of a single controlled segment.

Similarly to Eq. (25), the domain of the mode vector m of the whole model can be decomposed through the domains of all intercellular fluxes:

$$\mathrm{Dom}(m) = \bigcap_{i=0}^{N_s} Q_{i,i+1}. \tag{26}$$

In the following, the half-space representation of the polyhedron $P_m = \mathrm{Dom}(m)$ is given for all accepted modes. For the sake of generality, all possible mode vectors are considered ($m \in \{1,...,8\}^{N_s}$), and no restriction is given on the acceptable mode strings (i.e. no analysis is carried out on the impossible mode succession in the vector).

The polyhedra that represent the flux regions can be stated as intersections of three half spaces. Formally:

$$W_{i,i+1} = H_{i,i+1}^{\alpha} \bigcap H_{i,i+1}^{\hat{\beta}_b} \tag{27}$$

$$L_{i,i+1} = H^{\beta_a}_{i-1,i} \bigcap \overline{H^{\beta_b}_{i,i+1}} \tag{28}$$

$$D_{i,i+1} = \overline{H^{\alpha}_{i,i+1}} \bigcap \overline{H^{\beta_a}_{i-1,i}}, \tag{29}$$

where $H^{\alpha}_{i,i+1}$, $H^{\beta_a}_{i-1,i}$, $H^{\beta_b}_{i,i+1}$ are defined as

$$H^{\alpha}_{i,i+1} = \{\rho \in [0,\rho_{jam}] | \rho_{i+1} + \frac{\rho_{jam} + \rho_{b(i,i+1)}}{\rho_{a(i,i+1)}} \quad i = 0,...,N_s + 1\}, \tag{30}$$

$$H^{\beta_a}_{i,i+1} = \{\rho \in [0,\rho_{jam}] | \rho_i > \rho_{a(i,i+1)} \quad i = 0,...,N_s\}, \tag{31}$$

$$H^{\beta_b}_{i,i+1} = \{\rho \in [0,\rho_{jam}] | \rho_i > \rho_{b(i,i+1)} \quad i = 0,...,N_s\}, \tag{32}$$

whereas $\overline{H}$ denotes the complement of H.

As a conclusion, involving VSL control policy, the switching mode dependent CTM becomes control input triggered, i.e. we introduce u-dependency into the half-space representation of the operation modes as well as into the state dynamics. However, the model class remains a (parameter-dependent) piecewise affine system in the form PWA(u).

The outlined switching model relies on a polytopic representation of operation modes. This simple form serves as a basis for reachability analysis of system modes which is used in the controller design as well, detailed in the sequel.

4. Control design based on the VSL included CTM

In certain cases, a sudden growth of density may lead to backwards propagating, high density jamwaves. In the following, a coordinated VSL control design method is suggested that suppresses the shockwave formation and stabilizes network states by keeping traffic near critical conditions.

The controller is activated in case of shockwave is detected, similarly as in Hegyi et al. (2008). Control input values are chosen from a discrete set, matching realistic VSL control signs. By using the half-space representation of the switching mode model, the sequences are chosen to provide the largest number of *stable reachable modes*. Then, over the remaining set of sequences, a single-step optimization problem is solved aiming at network throughput maximization.

To support the controller design, first, the mode-reachability property is described. This is followed by the control framework and a clear algorithm for optimal control signal selection.

4.1. Reachable CTM modes

To support the VSL design, in the following, the one-step reachability property is analysed and later on adapted to controller design. As pointed out earlier, CTM modes depend on the chosen VSL signal. An important step in control design is to find a coordinated VSL control such that the reachable modes with stable states (see Remark 2) of the network are maximized.

To support this approach, first, polyhedral adjacency is defined (Thai and Bayen, 2015).

Definition 1. Two polyhedra P and P^* ($P,P^* \in \mathbb{R}^n$), are k-adjacent ($k \leqslant n$), if they have a facet of k dimension in common. Formally, this condition is satisfied if there is a supportive hyperplane H for the two polyhedra such that $P \bigcap P^* \bigcap H \in \mathbb{R}^k$.

The following assumption considers the smoothness of the system, i.e. with appropriately chosen sampling time and cell length the state trajectory will not skip the adjacent modes during one step.

Assumption 1. Let polyhedron $P_{m(k)} = Dom(m(k))$ represent mode $m(k)$, $P_{m(k)} \in \mathbb{R}^{N_s+2}$. In one discrete step, system modes can switch to the modes that have $N_s + 1$-adjacency of $P_{m(k)}$. The one-step accessible mode vectors $m^*(k)$ can be obtained by searching for all $(N_s + 1)$-adjacent polyhedra $P^*_{m(k)}$ of the current $P_{m(k)}$ polyhedron.

Example 1. As an illustrative example, consider $N_s = 1$. Then, $P_{m(k)} \in \mathbb{R}^3$ (see Fig. 7). In this case, the operation mode can be switched to modes whose polyhedra have two-dimensional adjacency with $P_{m(k)}$ through a facet (e.g. mode 1 can change to 2, 3, 5, but cannot change directly to modes 4, 6, 7, 8 as the polyhedra of these modes have no common facet with P_1).

The above assumption can be involved to VSL design by choosing the control signal such that the number of adjacent stable modes is maximized.

Remark 2. Here, stability is used in the traffic engineering sense, i.e. traffic density is below critical. Extending this notion to the case of VSL control, the mode is aimed that implies stability in cell i and its upstream cell, i.e. $\rho_i \leqslant \rho_{a(i,i+1)}$ and $\rho_{i-1} \leqslant \rho_{b(i-1,i)}$. This is satisfied by mode 7.

Remark 3. Reachability analysis can be expanded to multiple-step-ahead adjacency analysis, see Bemporad and Morari (1999). Note, however, that an analysis of a longer horizon requires a more thorough choice of sampling time than that of Assumption 1, where the sampling can be determined based on dynamical analysis. By choosing the sampling time too large, the number of reachable mode will explode; whereas choosing a too frequent sampling might impose infeasible requirements on the measurement and control system. Therefore, in the current paper, a one-step ahead analysis is followed, provided that Assumption 1 holds.

4.2. Receding horizon VSL coordination

In the sequel, a rolling horizon approach is proposed for coordinated VSL aiming at shockwave suppression. The selected framework is capable of addressing optimization problems under the mode dependent dynamics and input constraints. The control problem can be formalized generally, for prediction and control horizons (of length $N_{pr} > N_c$, respectively) as follows:

$$\min_{u} \quad \sum_{\ell=1}^{N_{pr}} \|Q((x(k+\ell|k) - r(k+\ell))\|_p + \|\varkappa(u(k+\ell) - u(k+\ell-1))\|_p \tag{33a}$$

subject to: Eq. (23) (33b)

$$u(k+\ell) \in \mathscr{U}, \quad \ell = 1,\ldots,N_c \tag{33c}$$

$$u_i(N_c+\ell) = v_f, \quad i = 1,\ldots,N_s \quad \ell = 1,\ldots,N_{pr}-N_c \tag{33d}$$

$$x(k+\ell|k) \in proj_x(\mathscr{P}_m^*), \quad \ell = 1,\ldots,N_{pr} \tag{33e}$$

with pre-selected weightings $Q \geq 0, \varkappa > 0$, $\|\cdot\|$ being the norm and $p = 1,2$ standing for the 1-, 2-norm. The optimization is subjected to hard constraints: apart from the equality constraint coming from the recursion of the input-dependent PWA model (described in Eq. (24)), input constraints are set for the VSL signal by means of spatial and other input consistency prescriptions. Furthermore, state constraints are considered for the one-step-ahead adjacency, Borrelli et al. (2011) and Bemporad and Morari (1999). Generally speaking, in (33a), capacity maximization is aimed over finite horizon by means of density tracking. We herewith define a reference tracking control policy, where $r(k+\ell)$ contains the mode dependent densities where segment capacity is maximized ($\rho_{a(i,i+1)}$, $i = 1,\ldots,N_s$).

By means of the adjacency analysis (see Remark 3), the reference signal creates a feasible trajectory. The solution to the optimization is a p-norm one subjected to nonlinear (input signal triggered) piecewise affine dynamics that fits into the framework of Mixed Integer Nonlinear Programming (MINLP) (Borrelli et al., 2011; Bemporad and Morari, 1999).

We propose a 2-stage online optimization problem in this vein (see Algorithm 1). In the first stage, the set of possible modes are reduced prior to the optimization. During Steps 1–6, all possible input and state constraints are computed. Spatial constraints are set on the VSL signal to limit differences between neighbouring segments and also to avoid spatial oscillation. Furthermore, a single-step analysis on stable reachable modes is used to reduce the set of the applicable input signals, preserving the ones that lead to the highest number of stable modes along the network.

Then, in Stage 2 (Step 8 in Algorithm 1), over the reduced set of input signals a Mixed Integer Nonlinear optimization is performed. The optimization problem can easily be solved in a relaxed way e.g. TOMLAB/MINLP resulting in optimal solution.

Steps are detailed in the sequel, giving a concise explanation to Algorithm 1.

Step 1 First, detection of shockwaves takes place. It is possible by using the threshold ρ_{th} for the density measurements of each segment. As a result of the detection, the extent (L_{jam}) and amplitude ($\rho_{i_{jam}}$) of the congestion is obtained. In case of no shockwave detection, the controller remains inactive and the algorithm returns to Step 1.

Step 2 In case of detecting a shockwave, first, the speed limit signal $vsl_{i_{jam}-1}$ upstream of the most congested segment is designed. It is selected such that the sending flow of the upstream segment is smaller than the receiving flow of the most congested segment. If the speed limit $vsl_{i_{jam}-1}$ is smaller than the lower bound of control input vsl_{min}, the lower bound is set as control input.

Step 3 Assuming jam solvability and consistency condition (i.e. the jamwave travels with a constant speed), coordinate VSL in the upstream of the detected bottleneck. To this end, the area of intervention $\mathscr{I}_{ctrl}$ is calculated as a function of the speed limit $vsl_{i_{jam}-1}$ and the extent of the jamwave L_{jam} (based on the results of Hegyi et al. (2008)).

Step 4 Construct the set of possible control input signals $\mathscr{U}$. Each element of the set $u \in \mathscr{U}$ consists of VSL values along the intervention area ($u = [vsl_i]$, $i \in \mathscr{I}_{jam}$). The elements of the input sequences are chosen from the discrete set of input signals vsl_{set}. Spatial constraints are formalized to limit input differences between adjacent segments and to exclude sequences with spatial oscillations, similarly as in Frejo et al. (2014).

Step 5 For the current polyhedron P_m and for each control sequence, find all adjacent modes P_{m^*}.

Step 6 Reduce the input set to $\mathscr{U}^{stable}$ by finding the control signals such that the number of segments is maximized for which stable modes in one step are reachable. For this, first calculate the number of stable modes (mode 7) for each P_{m^*}, given in $F(P_{m^*})$.

Step 7 Then, find control sequences that provide the highest number of stable reachable modes in the set $\mathscr{U}^{stable}$.

Step 8 The sequence leading to the best system performance is obtained by solving an optimization problem with of $\mathscr{U}^{stable}$. An N_{pr} long prediction is calculated with control horizon N_c, during which constant control input is given. The cost function includes the tracking problem for $\rho_a = [\rho_{a(i,i+1)}]$, $i = 1,\ldots,N_s$ (i.e. the density values, for which the capacity is maximal in

the VSL-controlled Godunov scheme) and the suppression of temporal oscillation of the input signal. This leads to the stabilization of the traffic network while the throughput is maximized.

The control design method is summarized in Algorithm 1.

Algorithm 1. VSL control design based on mode adjacency analysis

Stage 1

For all $\bigstar = \bigstar(k)$, $\bigstar^{+}/^{-} = \bigstar(k+1)/\bigstar(k-1)$:

1. Find $\mathscr{I}_{jam}$ such that for all $i \in \mathscr{I}_{jam}$ $\rho_i > \rho_{th}$, $L_{jam} = \sum_{i\in\mathscr{I}_{jam}} L_i$.
   $i_{jam} = \text{argmax}\, \rho_i$, $i \in \mathscr{I}_{jam}$.
   If $\rho_i \leqslant \rho_{th}$ $\forall$ i, return to Step 1.
2. Find $vsl_{i_{jam}-1}$ s.t. $S(\rho_{i_{jam}-1}, vsl_{i_{jam}-1}) \leqslant R(\rho_{i_{jam}}, vsl_{i_{jam}})$.
   If $vsl_{i_{jam}-1} < vsl_{min}$, $vsl_{i_{jam}-1} = vsl_{min}$.
3. Calculate $L_{ctrl} = f(L_{jam}, vsl_{i_{jam}-1}, \rho_{i_{jam}})$ and $\mathscr{I}_{ctrl}$ such that $L_{ctrl} = \sum_{i\in\mathscr{I}_{ctrl}} L_i$.
4. Specify $u \in \mathscr{U}$, $u = [vsl_i]$, $i \in \mathscr{I}_{ctrl}$ s.t. $vsl_i \in vsl_{set}$ and

$$\hat{u} = \begin{cases} vsl_i - vsl_{i-\ell} > 0 \;\; and \;\; vsl_i - vsl_{i+1} > 0, & \ell = \{1,2\} \\ vsl_i - vsl_{i-\ell} < 0 \;\; and \;\; vsl_i - vsl_{i+1} < 0, & \ell = \{1,2\} \end{cases}, \qquad \mathscr{U} = \mathscr{U} \setminus \hat{u}$$

5. For $P_m \in \mathbb{R}^{N_s+2}$ and $u \in \mathscr{U}$ find all adjacent modes $P_{m^*} \in \mathbb{R}^{N_s+2}$ and define the triplet $\Gamma = (P_m, u, P_{m^*})$ $P_m, P_{m^*} \in \mathbb{R}^{N_s+2}, u \in \mathscr{U}$
6. $F: \mathbb{R}^{N_s+2} \to \mathbb{Z}$: $F(P_{m^*}) = \sum_i C^i_{m^*}$, $C^i_{m^*} = \begin{cases} 1, & if \;\; m^*_i = 7 \\ 0, & else \end{cases}$
7. $\mathscr{U}^{stable} = \{\text{argmax}_u \{F(P_{m^*}) | (P_m, u, P_{m^*}) \in \Gamma\}\}$

Stage 2

8. Find optimal u^*:

$$\min_{u^*} \quad \sum_{\ell=1}^{N_{pr}} \|Q(x(k+\ell) - \rho_a(k+\ell))\|_2 + \|R(u(k+\ell) - u(k+\ell-1))\|_2 \tag{34a}$$

$$\text{subject to:} \quad x(k+1) = A_1^{m(k)}(u(k))x(k) + A_0^{m(k)}(u(k)) + H_1^{m(k)}(u(k))d(k) \tag{34b}$$

$$u^* \in \mathscr{U}^{stable} \quad \ell = 1,\ldots,N_c \tag{34c}$$

$$u(k+\ell) = u^* \quad \ell = 1,\ldots,N_c \tag{34d}$$

$$u_i(N_c+\ell) = v_f \quad i = 1,\ldots,N_s \quad \ell = 1,\ldots,N_{pr}-N_c \tag{34e}$$

Remark 4. It is important to notice that the optimization of Stage 2 is run on a significantly reduced set of input signals as a result of the adjacency analysis (by choosing $\mathscr{U}^{stable}$ as $\mathscr{U}$ in Eq. (34c) according to Steps 6–7). Consequently, the number of decision variables during the optimization is significantly reduced.

Remark 5. In Section 5, $p = 2$ with $Q_i = TL_i$, $R = I_{N_s\times N_s}$ is used resulting in a quadratic cost i.e. a 2-norm optimization for mode dependent density tracking of $\rho_{a(i,i+1)}$, $i = 1,\ldots,N_s$. Following a manual tuning, a prediction horizon $N_{pr} = 10$ and control horizon $N_c = 4$ is chosen for the adjacency-based controller. (Further analysis of the prediction and control horizons is given in Section 5.4.)

5. Simulation analysis

In the sequel, the previously proposed VSL control policy (referred to as adjacency-based VSL) is tested in two case studies through a comparison of two alternative VSL control strategies: (i) the method SPECIALIST (Hegyi et al., 2008) and (ii) a model predictive controller (MPC) based on the works of Hadiuzzaman and Tony (2013), Frejo et al. (2014), adapted to the problem as shown in B. Methods are chosen such that they share similar model frameworks: SPECIALIST uses the shockwave theory with the triangular fundamental diagram for tuning the controller. However, it does not use CTM for dynamic recursion. The MPC applies CTM in its original form, addressing the nonlinearities coming from the minimum conditions of the Godunov flows by the nonlinear model predictive control scheme, Grüne and Pannek (2011). Although it is tuned with similar control parameters as the adjacency-based approach, it has no triggering conditions and works with a quadratic reference tracking objective.

Table 3
Model parameters.

Parameter	Value
v_f	80 km/h
w	−26.67 km/h
ρ_{cr}	30 veh/km/lane
ρ_{th}	45 veh/km/lane
ρ_{jam}	120 veh/km/lane
λ_i (No. of lanes)	1 $\forall$ i
vsl_{set}	{40,50,60,70,80} km/h
N_s (case study 1)	16
N_s (case study 2)	38
T	30 s
L_i	1 km $\forall$ i
Sim. time	120 min

Simulations are run in Matlab for 16 km/38 km long single-lane motorway test systems, assuming the model parameters are as in Table 3. These parameters are chosen to describe a realistic motorway arterial. Jam density parameter is chosen intentionally high, to avoid too large capacity reduction by VSL. The strictest control (i.e. 40 km/h) regulates a capacity reduction of 20%. A lower jam density would impose a steeper slope of w, and hence a more significant capacity reduction could be reached via VSL signs.

The case studies are analyzed through space-time plots of the commanded control signal, the traffic density and the corresponding traffic speed values. The evaluation is also carried out by means of network aggregated variables, following the traffic stream definitions of Edie (1965):

- *Total time spent (TTS)* is obtained as follows

$$TTS = \sum_{k=1}^{K} \sum_{i=1}^{N_s} \lambda_i \rho_i(k) L_i T, \tag{35}$$

where K denotes the analyzed time domain (in our case the simulation time).

- *Total travel distance (TTD)* represents the effective capacity of the system. It is presented in the form

$$TTD = \sum_{k=1}^{K} \sum_{i=1}^{N_s} \lambda_i G(\rho_i(k),\rho_{i+1}(k)) L_i T, \tag{36}$$

where $G(\rho_i,\rho_{i+1})$ denotes the per lane outflow from segment i, calculated as in Eq. (22). By this formula, trip completion for segment i is expressed by means of its outflow and its length L_i. The same metrics are adopted in a normalized form in Schmitt et al. (2015), Gomes and Horowitz (2006).

- *Network average speed*, obtained as the quotient of the travelled distance and the time spent in network:

$$\bar{v} = \frac{TTD}{TTS}. \tag{37}$$

The *throughput capacity* of the network is the total number of vehicles that complete the whole network during the simulation. Since the simulation horizon is long enough that all vehicles that are initially present leave the network during the simulation, the value can be given by the following formula:

$$TC = T \sum_{k=1}^{K} \lambda_i G(\rho_0(k),\rho_1(k)) - \sum_{i=1}^{N_s} \lambda_i \rho_i(K) L_i, \tag{38}$$

i.e. the sum of total inflow minus the number of vehicles that remain in the network in the final simulation step K.

Furthermore, to quantify the duration of traffic jams, *settling time* is given. Settling of a traffic jam is considered if traffic density falls below a threshold value on the whole network after VSL activation. The threshold is chosen as $\rho_{cr}(vsl)|_{vsl=70} = 33.103$ veh/km/lane. This assumption means that traffic is stable in case of the mildest control, VSL = 70 km/h.

5.1. Suppression of short jamwaves

In the first case study the three controllers are tested on a two-hour-long rush hour scenario. The aim is to analyse the behaviour of the controller during shockwave suppression. To emulate saturated traffic conditions, at the boundaries, critical density is set throughout the simulation. Network load and disturbances are chosen such that short jamwaves are triggered which meet at a certain point and a short but high intensity shockwave is emulated.

The shockwaves are created by giving disturbances as additional density $\Delta\rho$ for a short period of time to mimic sudden density

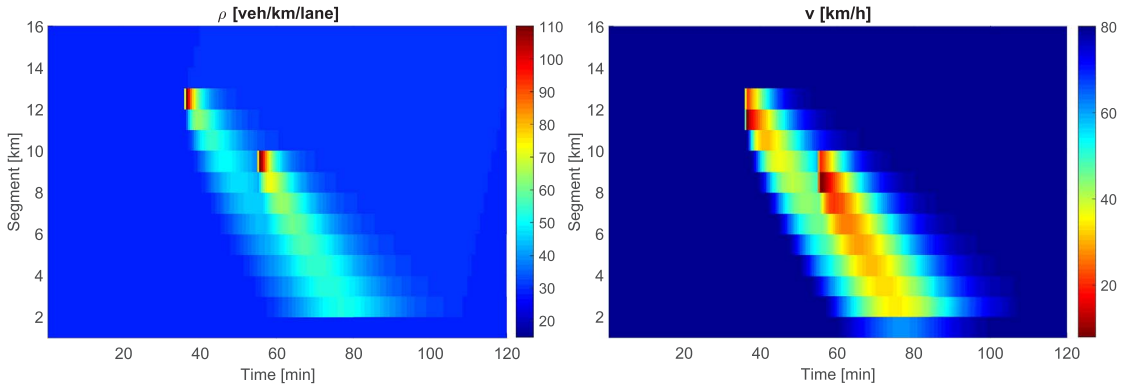

Fig. 8. Case of no control.

growth. These high density areas are allocated at segments 9 and 13, with additional densities $\Delta\rho_{13}(t)|_{t=[36]\,\mathrm{min}} = 40$ veh/km/lane and $\Delta\rho_{9}(t)|_{t=[55]\,\mathrm{min}} = 40$ veh/km/lane.

In Fig. 8, the density and speed profiles of the uncontrolled scenario are depicted. The effect of the disturbances can be clearly seen: from segment No. 13 a shockwaves arises which reaches the other shockwave, started at segment No. 9, leading to a high-density and low speed area, upstream from segment No. 9.

Among the controllers, first, the results of the MPC algorithm are analyzed (see Fig. 10). The shockwave is suppressed, by applying moderate VSL restriction in an extensive manner both in space and time (for 11 km and 40 min, see Fig. 9), which eventually eases the second shockwave by restricting flows upstream of segment No. 9 in advance. Also, some oscillation appears around 50 and 65 min. VSL signs are given in cases if no congestion appears (e.g. at 70 min, downstream of the jamwave). This VSL activation is due to the quadratic density error minimization framework. MPC aims to compensate the low density areas of forward propagating waves, too.

The controller SPECIALIST requires the pre-selection of the VSL signals, which may be tuned to the amplitude of the shockwave. The controller performed the best when choosing VSL = 50 km/h. At the upstream bound of the VSL area a two-cell-long transition zone is given by 70 km/h and 60 km/h signals. The extent the intervention zone is proportional to the jamwave amplitude and length, thus the second jamwave is addressed by the same VSL restriction zone as shown in Fig. 11. The method suppressed the jamwaves effectively with a very short density peak (Fig. 12a), however, by a use of an extensive VSL intervention area.

The adjacency-based VSL controller results are shown in Figs. 13 and 14. Regarding the control input values (Fig. 13), no spatial oscillation of VSL signals appears. However, a slight temporal oscillation at the second shockwave can be observed (segment No. 5 at 59 min). With the proposed method, the advantage of dynamic VSL coordination is visible. In the upstream proximity of the bottleneck, VSL speed restriction is significant. The rest of the cells' VSL signal is however selected in a monotonically decreasing way.

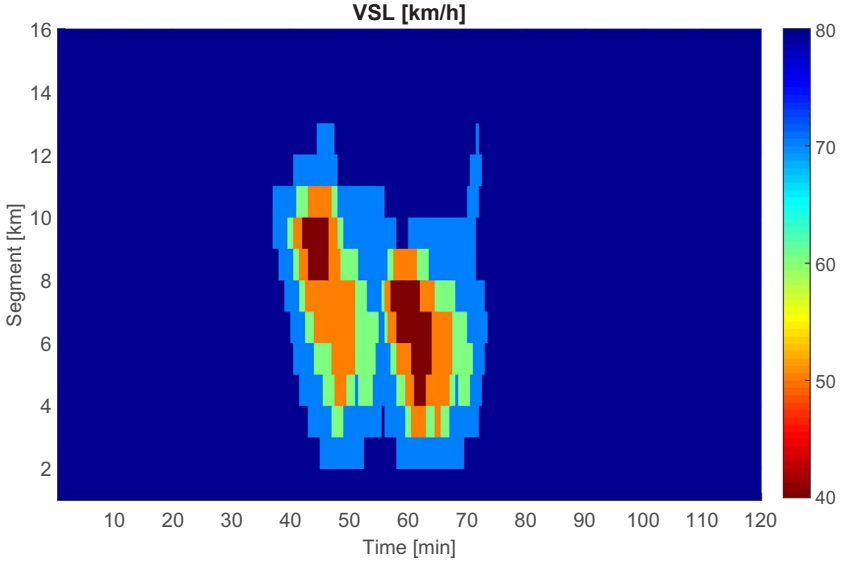

Fig. 9. Control input of the MPC approach.

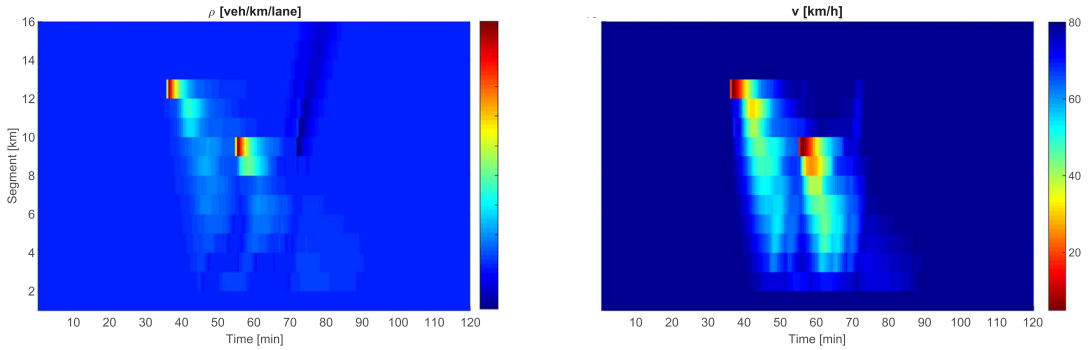

(a) Density profile (b) Speed profile

Fig. 10. MPC control.

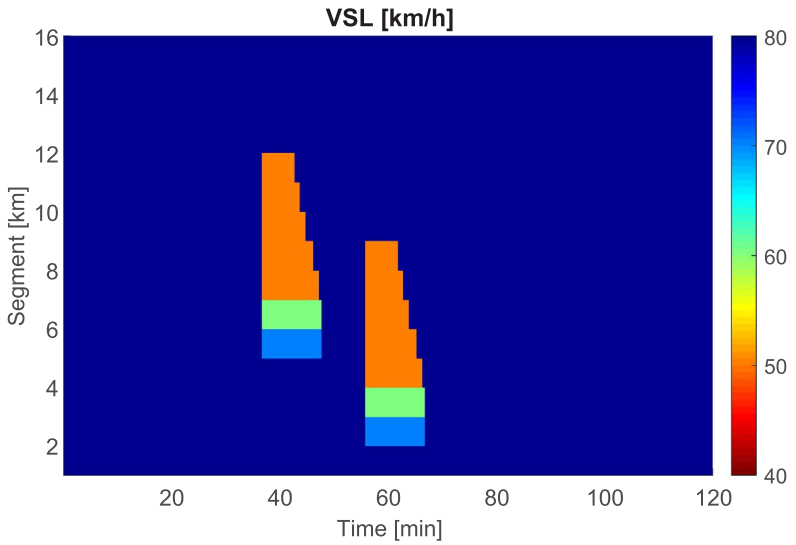

Fig. 11. Control input of SPECIALIST.

Finally, whenever the congestion is alleviated, speed limits are stopped being activate.

Among the three controllers, the SPECIALIST reached the lowest TTS value and the fastest settling times (see Table 4). However, this is a result of a constant VSL value of an extensive zone upstream of the bottleneck. This leads to a sub-utilization of the network downstream of the bottleneck and low overall TTD and throughput performance. The MPC uses a large spatiotemporal domain for

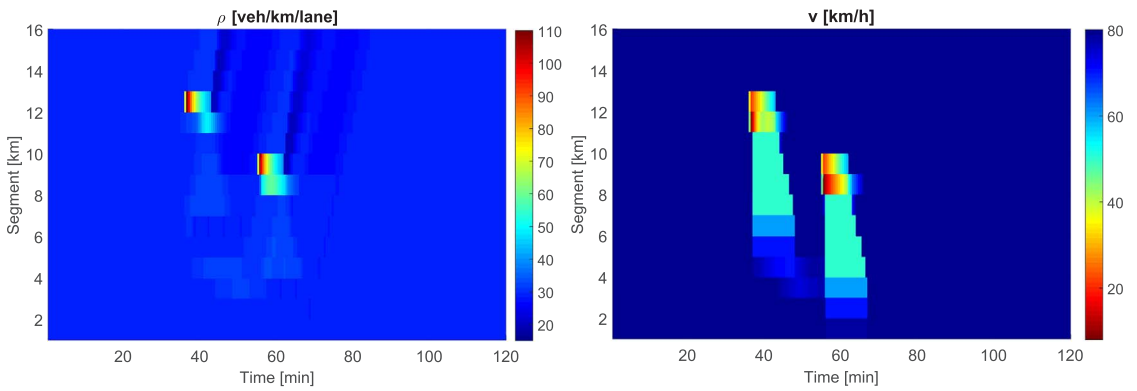

(a) Density profile (b) Speed profile

Fig. 12. SPECIALIST control.

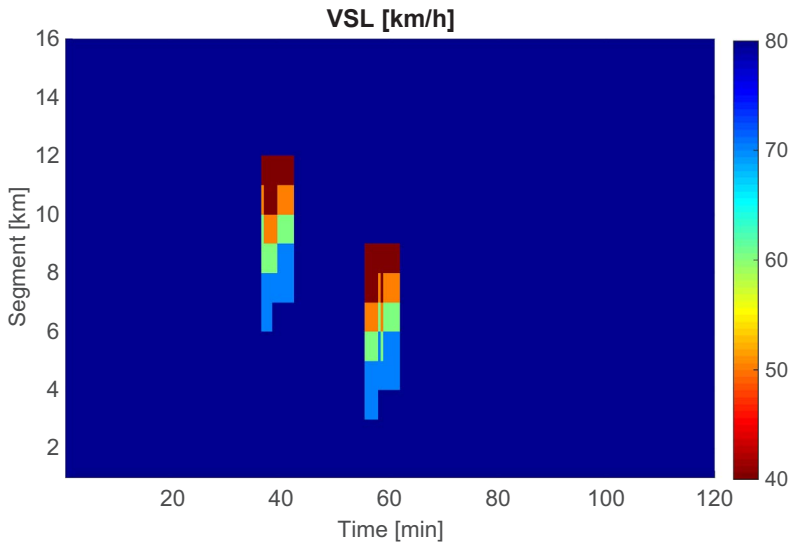

Fig. 13. Control input of the adjacency-based controller.

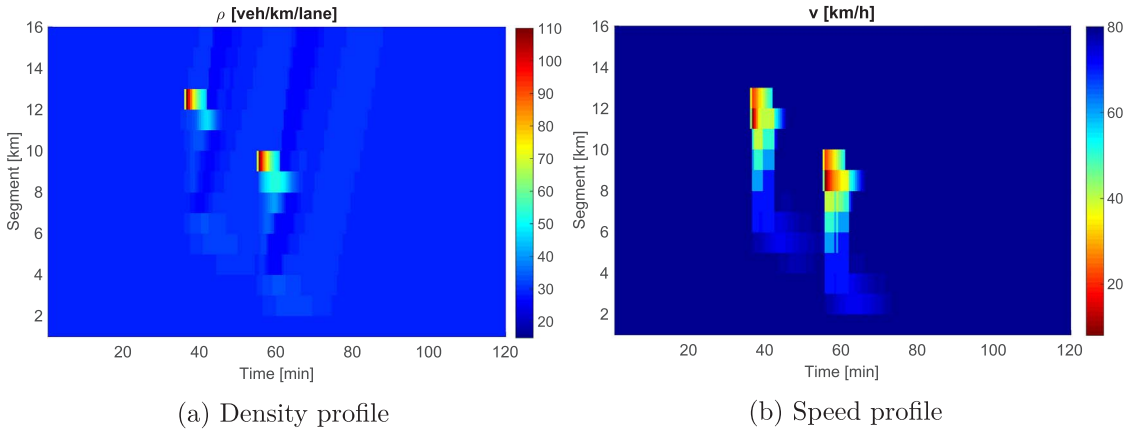

Fig. 14. Adjacency-based control.

VSL activation, and although it suppresses the shockwave, it does not provide as fast response as the SPECIALIST or the adjacency-based controller. The latter approach applies low VSL values for a fast stabilization of the system, whereas control activation is restricted to a small spatiotemporal area. This is a result of the adjacency analysis which leads to an effective reduction of the control signal set. Nevertheless, all three controllers lead to an improvement in network average speed and throughput capacity, (the adjacency-based controller providing the highest values).

Table 4
Aggregated results of case study 1.

	Uncontrolled	MPC	SPECIALIST	Adj. based
TTS [veh h]	1037.9	973.2	949.27	956.34
TTD [veh km]	73857.1	73984.2	72945.3	74560.0
$\bar{v}$ [km/h]	71.17	76.01	76.84	77.97
TC [veh]	4109.0	4225.3	4252.8	4257.7
Settling time [min] - 1st shockwave	–	19	19	18
Settling time [min] - 2nd shockwave	–	17	14	19

5.2. Handling of extensive jams

In the second case study an extensive traffic jam is considered: a 3 km long jamwave. This scenario aims at showing the benefits of handling spatially extensive traffic jams, i.e. scalability of algorithms with appropriate performance.

The uncontrolled case is plotted in Fig. 15. The wide moving jam lasts for almost two hours, ranging up to 20 km.

MPC results in an acceptable performance in attenuating the moving jam (see Fig. 17a), again, by applying moderate input in an extensive spatiotemporal activation domain (as shown in Fig. 16: for around 25 min and 10 km). After suppressing the shockwave, further VSL restriction zones can be seen both upstream and downstream of the original jam, which lead to a sub-utilization of the network (see Fig. 18).

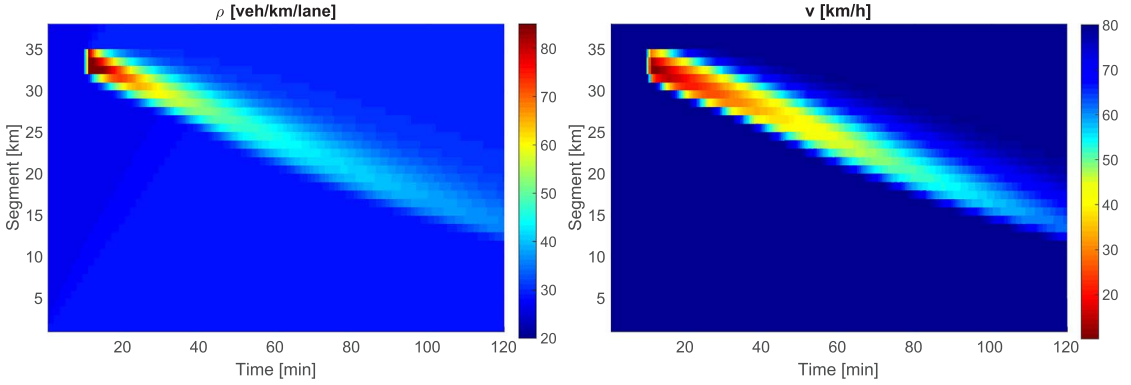

(a) Density profile (b) Speed profile

Fig. 15. Case of no control.

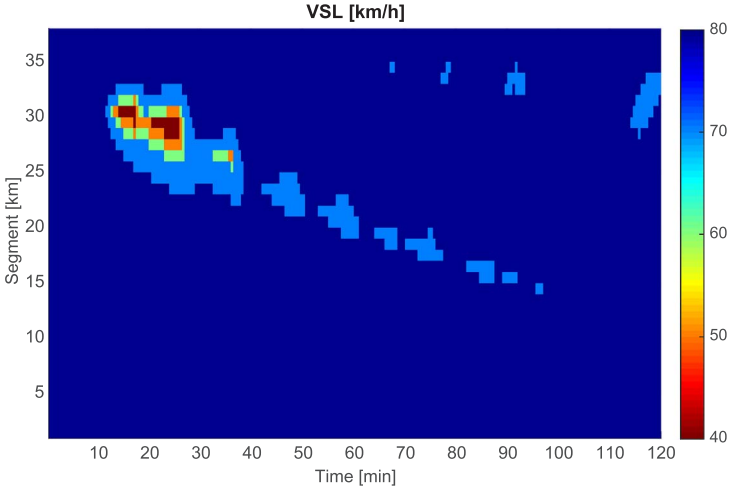

Fig. 16. Control input of MPC.

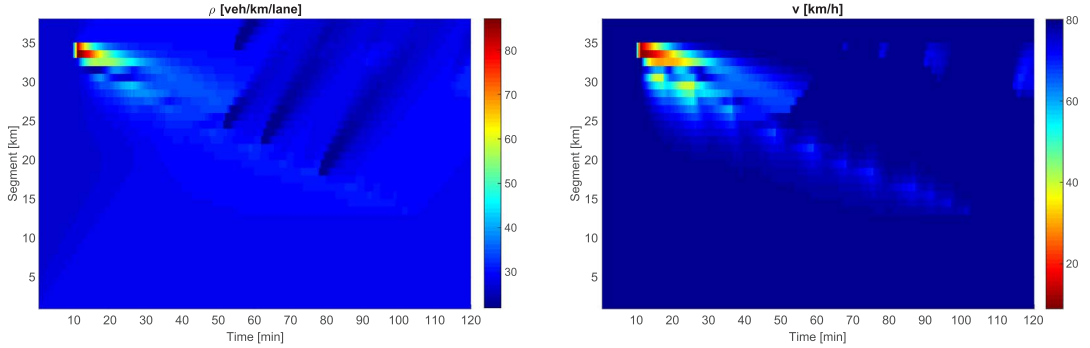

(a) Density profile (b) Speed profile

Fig. 17. MPC approach.

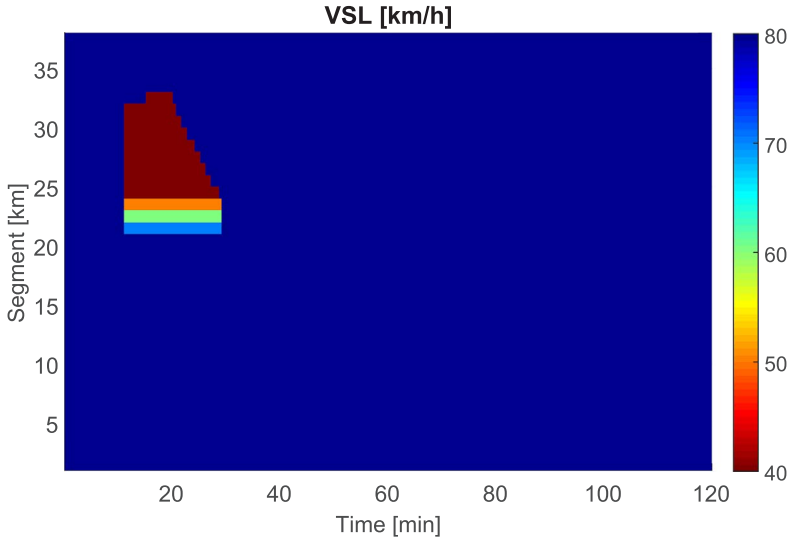

Fig. 18. Control input of SPECIALIST.

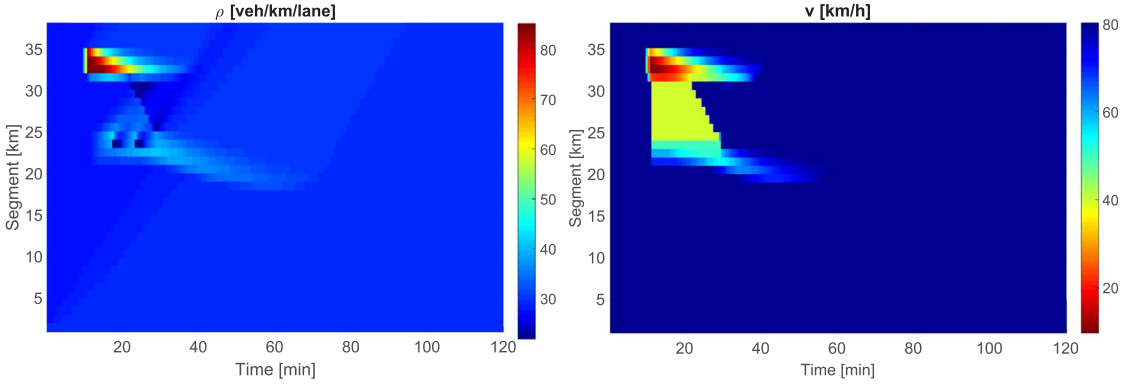

(a) Density profile (b) Speed profile

Fig. 19. SPECIALIST control.

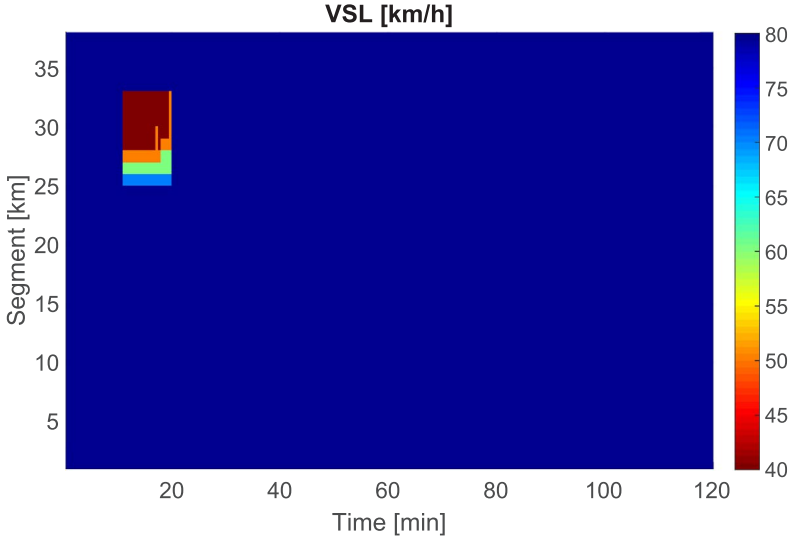

Fig. 20. Control input of adjacency-based control.

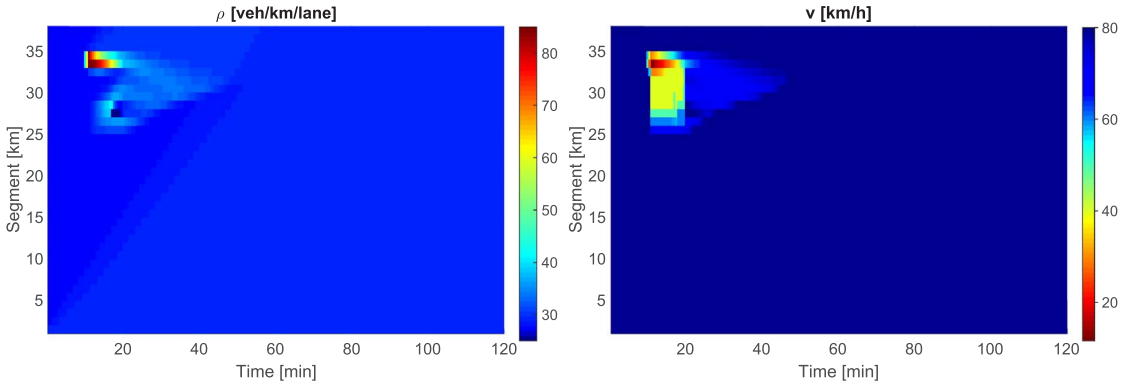

Fig. 21. Adjacency-based control.

Table 5
Aggregated results of case study 2.

	Uncontrolled	MPC	SPECIALIST	Adj. based
TTS [veh h]	2504.7	2287.6	2293.4	2286.9
TTD [veh km]	172028.3	172238.4	172463.3	174719.1
$\bar{v}$ [km/h]	68.68	75.29	75.20	76.39
TC [veh]	3535.7	3583.9	3591.3	3591.3
Settling time [min]	–	55	53	51

The SPECIALIST approach provides a good overall performance, effectively suppressing the jamwave. However, in this scenario, different from the first one, VSL = 40 km/h value is selected (Fig. 19). With 50 km/h the jam was judged as unsolvable. This shows the sensitivity of the SPECIALIST controller to the jam conditions and parameter tuning. Finally, the large spatiotemporal extent of VSL activation implies a rather conservative solution.

The adjacency-based controller performs similar to the SPECIALIST, however, with a much smaller activation domain. While the MPC and the SPECIALIST approaches triggered other, smaller amplitude jamwaves at the tail of their activation zone, the adjacency-based controller avoids this effect. Compared to the MPC control, it stabilizes the system in a fast and effective manner (see Figs. 20 and 21).

Aggregated variables are summarized in Table 5. SPECIALIST and the adjacency-based controller reach similar closed loop performances in terms of TTS and the throughput capacity as well. It is important to note though, that the network capacity is exploited at the highest level by the adjacency-based control, providing both an improvement in network average speeds and an increase in the distance travelled. Furthermore, the proposed technique is minimalistic in the sense of using VSL control resources (among the three candidates, it is activated over the smallest spatiotemporal domain).

5.3. Computational demand

The proposed VSL approach does not only return with good network performance, but also with low CPU time,[5] see Table 6 where computation times of steps with active control are given. In terms of computational needs, due to the simple PWA dynamics, the proposed controller lies in between the cheap SPECIALIST having no dynamic recursion and the expensive MPC solution that realizes nonlinear recursion.

Table 6
Average computation time/step [s] for active VSL control.

Case study no.	MPC	SPECIALIST	Adj. based
1	2.005	0.0018	0.019
2	5.308	0.0026	0.884

[5] Run on an Intel i5 3.0 GHz, 8 GB RAM computer.

The computational demand of the adjacency-based VSL control depends primarily on the spatial extent of control input (the number of cells to coordinate) and secondarily on the prediction horizon of the optimization in Stage 2. In terms of cell coordination, VSL control is only active for a limited number of segments upstream of the traffic jam (e.g. in the first case study VSL is activated for 6 segments whereas in the second one for 8 segments). Following the exclusion of non-desired input behaviour, a limited number of possible input signals remain (on average, in each step 15 and 70 input signals remain for case studies 1 and 2, respectively). For each of the remaining signals, the one-step reachable mode vectors are calculated (in the first case, a maximum of 42 and in the second, a maximum of 56 reachable modes can be considered). By analysing the reachable modes, the set of input signals is further reduced to the ones that maximize the number of cells with stable adjacent modes. During the optimization of Stage 2, constant VSL control is assumed for the control horizon.

However this structure lowers the computational demand, the increase of the controlled zone entails an explosion of possible VSL sequences and consequently, CPU time. This problem can be avoided by choosing appropriate spatial sampling, or in case of a fine spatial discretization, a grouping of neighbouring cells is advised.

5.4. Analysis of the prediction horizon

As highlighted, the suggested algorithm provides a significant reduction in decision variables compared to the pure MPC approach, where the VSL of each controlled cell is used as a decision variable. In Table 7 it is also shown, that by increasing the prediction horizon the change in CPU times is negligible. This is a clear consequence of the algorithm: the computational effort is focused on calculating and reducing the set of VSL signals during the adjacency analysis; then, the optimization is albeit run for a finite horizon during the prediction, a frozen VSL signal is used for $N_c < Np$.

The different control horizons show very close values in TSN performance. This similarity highlights that once the set of possible VSL signals is reduced to those stabilizing the network for the most segments, a good overall performance can be reached.

Table 7
Comparison of prediction horizons.

Case study 1			Case study 2		
N_p	Avg. CPU time/step [s]	$\bar{v}$ [km/h]	N_p	Avg. CPU time/step [s]	$\bar{v}$ [km/h]
1	0.0071	75.47	1	0.817	75.22
2	0.0088	75.40	2	0.823	75.22
3	0.0099	75.86	3	0.834	75.74
4	0.0117	77.59	4	0.840	75.86
5	0.0129	77.71	5	0.842	75.98
6	0.0148	77.71	6	0.849	76.12
7	0.0160	77.78	7	0.853	76.29
8	0.0171	77.89	8	0.866	76.35
9	0.0186	77.93	9	0.872	76.37
10	0.0194	77.97	10	0.884	76.39

6. Summary and future directions

In this paper, a mode dependent variable speed limit (VSL) strategy for network motorway control is developed. The suggested coordinated flow control algorithm is based on a switching mode formalization of the Cell Transmission Model (CTM). First, the effect of VSL is included in CTM creating a novel feasible mode model. Although the CTM with VSL belongs to the Piecewise Affine (PWA) model class, the mode dynamics is shown to be parameter dependent. Given a half-space representation of the mode dependent and scheduled polyhedra, reachable and stable modes are characterized. In this vein, a coordinated VSL solution is proposed. The set of possible VSL sequences is created by applying physical constraints to eliminate spatial and temporal oscillations. Then, the set is reduced according to stable reachable modes of the switching system. Over the remaining set of sequences, a capacity maximization problem is solved that is classified as a mixed integer optimization problem with linear cost function subjected to nonlinear constraints. The method is implemented in simulation environment to show its viability in shockwave suppression.

The proposed system, however, has its limitations. Since the switching system has eight feasible modes, for an N_s-dimensional system, the cardinality of the mode vectors mounts to 8^{N_s}, which may drastically increase computational burden. In the proposed controller setup, this is simplified by using a receding horizon control based on a single-step adjacency analysis. Another interesting research direction is the control design of parameter dependent PWA systems, considering the input-dependence of the polyhedral representation of system modes. The applied traffic modelling framework can also be improved. The basic CTM does not take into account the capacity drop. The phenomenon, however, can be involved to the model by defining the sending flow function as $S = q_c^{drop} < q_c$ for $\rho > \rho_{cr}$ instead of q_c, or a density dependent form, e.g. $S = q_c^{drop}(\rho)$, see Han et al. (2017). Apart from the slightly different dynamics, this modification entails further changes in the number of modes and the switching conditions which needs to be addressed carefully.

Furthermore, the proposed scheme is applied for motorway arterials with no on- or off-ramps, the involvement of which leads to a more general description of motorway network. However, the comprehensive formalization of merging conditions of ramps with the presence of VSL control leads to a very different and also, extensive model, described by merging rules. In this case, although the system dynamics remain affine by involving controlled on-ramps, additional non-trivial merging conditions need to be considered in the Godunov schemes (see e.g. Ferrara et al., 2015). A possible future research direction points at providing a similar, PWA-based form, also involving the merging conditions at ramps.

Acknowledgements

This research is supported by Chalmers' initiatives in transport research, the Transport Area of Advance at Chalmers University of Technology and SAFER (Vehicle and Traffic Safety Centre) and by the National Research, Development and Innovation Office of Hungary - NKFIH through Grant No. 115694. B. Kulcsar gratefully acknowledges the support received from Aeje.

Appendix A

Proof of Proposition 1. Let the possible VSL relations for three subsequent segments be denoted by A ($vsl_i > vsl_{i+1}$) and B ($vsl_i \leqslant vsl_{i+1}$). Then, a total of four cases needs to be examined (see Table 8).

In what follows, the definitions of ρ_a and ρ_b in cases A and B (given in Table 9) are compared for each case.

Table 8
Input relation cases.

Case	vsl_{i-1} vs. vsl_i	vsl_i vs. vsl_{i+1}
1	A	A
2	A	B
3	B	A
4	B	B

Table 9
ρ_a, ρ_b definitions.

Relation	$\rho_{a(i,i+1)}$	$\rho_{b(i,i+1)}$
A	$\frac{\rho_{cr}(vsl_{i+1})vsl_{i+1}}{vsl_i}$	$\rho_{cr}(vsl_{i+1})$
B	$\rho_{cr}(vsl_i)$	$\rho_{cr}(vsl_i)$

Case (1)

$$\rho_{b(i-1,i)} = \frac{\rho_{jam} w}{w + vsl_i} \tag{A.1}$$

$$\rho_{a(i,i+1)} = \frac{\rho_{jam} w}{w + vsl_i} \frac{vsl_{i+1}}{vsl_i} \tag{A.2}$$

Assume $\rho_{b(i-1,i)} > \rho_{a(i,i+1)}$. Substituting (A.1) and (A.2):

$$\frac{\rho_{jam} w}{w + vsl_i} > \frac{\rho_{jam} w}{w + vsl_i} \frac{vsl_{i+1}}{vsl_i} \tag{A.3}$$

$$vsl_i > vsl_{i+1}, \tag{A.4}$$

which satisfies the assumption.

Case (2)

$$\rho_{b(i-1,i)} = \rho_{cr}(vsl_i) \tag{A.5}$$

$$\rho_{a(i,i+1)} = \rho_{cr}(vsl_i) \tag{A.6}$$

Therefore, the assumption $\rho_{a(i,i+1)} \leqslant \rho_{b(i-1,i)}$ holds.

Case (3)

$$\rho_{b(i-1,i)} = \frac{\rho_{jam} w}{w + vsl_{i-1}} \tag{A.7}$$

$$\rho_{a(i,i+1)} = \frac{\rho_{jam} w}{w + vsl_{i+1}} \frac{vsl_{i+1}}{vsl_i} \tag{A.8}$$

Assume $\rho_{b(12)} > \rho_{a(23)}$. Substituting (A.7) and (A.8):

$$\frac{\rho_{jam} w}{w + vsl_1} > \frac{\rho_{jam} w}{w + vsl_3} \frac{vsl_3}{vsl_2} \tag{A.9}$$

$$vsl_2 > vsl_3 \tag{A.10}$$

Since $vsl_i > vsl_{i+1}$, LHS (A.9) > 0. Also, as $vsl_{i-1} \leqslant vsl_i$, RHS (A.9) $\leqslant 0$. Therefore, $\rho_{a(i,i+1)} \leqslant \rho_{b(i-1,i)}$ is satisfied.

Case (4)

$$\rho_{b(i-1,i)} = \frac{\rho_{jam} w}{w + vsl_{i-1}} \tag{A.11}$$

$$\rho_{a(i,i+1)} = \frac{\rho_{jam} w}{w + vsl_i} \tag{A.12}$$

The case condition $vsl_1 \leqslant vsl_2$ entails the satisfaction of $\rho_{a(23)} \leqslant \rho_{b(12)}$. □

Appendix B. MPC control

The following optimization problem is considered:

$$\min_{u} \quad \sum_{\ell=1}^{N_{pr}} \sum_{i=1}^{N_s} \|Q_i((\rho_i(k+\ell|k) - r_i(k+\ell))\|_2^2 + \sum_{\ell=1}^{N_c} \|\kappa_t(u(k+\ell) - u(k+\ell-1))\|_2^2 \tag{B.1a}$$

$$\text{subject to:} \quad \rho_i(k+1) = \rho_i(k) + \frac{T}{L_i}(\min(S_{i-1}(k), R_i(k)) - \min(S_i(k), R_{i+1}(k))) \tag{B.1b}$$

$$S_i(k) = \min\left(\rho_i(k) vsl_i(k), \frac{\rho_{jam} w}{(w + vsl_i(k))} \max\left(1, \frac{vsl_{i+1}(k)}{vsl_i(k)}\right)\right) \quad i = 1,\ldots,N_s$$

$$R_i(k) = \min\left(-w(\rho_i(k) - \rho_{jam}), \frac{\rho_{jam} w}{(w + vsl_i(k))} \max\left(1, \frac{vsl_{i+1}(k)}{vsl_i(k)}\right)\right) \quad i = 1,\ldots,N_s$$

$$d(k+\ell) = d(k), \quad \ell = 1,\ldots,N_{pr} \tag{B.1c}$$

$$vsl_i(k+\ell) \in \{vsl_{set}\}, \quad i = 1,\ldots,N_s, \quad \ell = 1,\ldots,N_c \tag{B.1d}$$

$$vsl_i(k+\ell) - vsl_{i+1}(k+\ell) \leqslant \Delta_{vsl,max} \quad i = 1,\ldots,N_s - 1, \quad \ell = 1,\ldots,N_c \tag{B.1e}$$

$$vsl_i(k+\ell) = v_f \quad i = 1,\ldots,N_s, \quad \ell = N_c + 1,\ldots,N_{pr} \tag{B.1f}$$

where $Q_i = TL_i$, κ_t is the weighting factor for suppressing and temporal input oscillations (for the case study, $\kappa_t = 0.1$ is chosen). The reference signal in this case is given as $r_i = \rho_{a(i,i+1)}$, $i = 1,\ldots,N_s$ to maximize outflow performance.

Optimization problem (32a)–(32d) is adapted to the MPC framework following the control design as shown in Hadiuzzaman and Tony (2013). The dynamic equations involving the minimum conditions of the Godunov scheme and the VSL control model are put as equality constraint for recursion (B.1b). Furthermore, an equality constraint is involved for the disturbance: throughout the control horizon, the measured disturbance is considered constant (B.1c). Spatial constraints on the input are defined as in Frejo et al. (2014): the differences between the adjacent segments are bounded too with $\Delta_{vsl,max} = 10$ km/h.

The controller solves the optimization problem in a rolling horizon fashion, see Grüne and Pannek (2011). For the case studies, a control horizon of $N_c = 5$ and prediction horizon $N_{pr} = 10$ are applied.

References

Bemporad, A., Morari, M., 1999. Control of systems integrating logic, dynamics and constraints. Automatica 35 (3), 407–427.

Borrelli, F., Bemporad, A., Morari, M., 2011. Predictive Control for Linear and Hybrid Systems. Cambridge University Press.

Canudas De Wit, C., Leon Ojeda, L.R., Kibangou, A.Y., 2012. Graph constrained - CTM observer design for the Grenoble South Ring. In: 13-th IFAC Symposium on Control in Transportation Systems. Sofia, Bulgaria.

Courant, R., Friedrichs, R.K., Lewy, H., 1928. Über die Partiellen Differenzengleichungen der mathematischen Physik. Mathematische Annalen 100, 32–74.

Daganzo, C.F., 1994. The cell transmission model: a dynamic representation of highway traffic consistent with the hydrodynamic theory. Transport. Res. Part B: Methodol. 28 (4), 269–287.

Edie, L.C., 1965. Discussion of traffic stream measurements and definitions. In: Proceedings of the 2nd International Symposium on the Theory of Traffic Flow, Organisation for Economic Co-operation and Development. pp. 139–154.

Ferrara, A., Sacone, S., Siri, S., 2015. A switched ramp-metering controller for freeway traffic systems. IFAC-PapersOnLine 48 (27), 105–110.

Frejo, J.R.D., Nunez, A., Schutter, B.D., Camacho, E.F., 2014. Hybrid model predictive control for freeway traffic using discrete speed limit signals. Transport. Res. Part C: Emerg. Technol. 46, 309–325.

Godunov, S., 1959. A finite difference method for the numerical computation of discontinuous solutions of the equations of fluid dynamics. Math. Sbornik 47, 271–306.

Gomes, G., Horowitz, R., 2006. Optimal freeway ramp metering using the asymmetric cell transmission model. Transport. Res. Part C: Emerg. Technol. 14 (4), 244–262.

Gomes, G., Horowitz, R., Kurzhanskiy, A.A., Varaiya, P., Kwon, J., 2008. Behavior of the cell transmission model and effectiveness of ramp metering. Transport. Res. Part C: Emerg. Technol. 16 (4), 485–513.

Greenshields, B.D., 1935. A study of traffic capacity. In: Proceedings of the Highway Research Board, vol. 14, pp. 448–477.

Grüne, L., Pannek, J., 2011. Nonlinear Model Predictive Control: Theory and Algorithms. Springer, London.

Hadiuzzaman, M., Tony, Z.Q., 2013. Cell transmission model based variable speed limit control for freeways. Can. J. Civil Eng. 40 (1), 46–56.

Han, Y., Hegyi, A., Yuan, Y., Hoogendoorn, S., 2017. Validation of an extended discrete first-order model with variable speed limits. Transport. Res. Part C: Emerg. Technol. 83, 1–17.

Han, Y., Hegyi, A., Yuan, Y., Hoogendoorn, S., Papageorgiou, M., Roncoli, C., 2017. Resolving freeway jam waves by discrete first-order model-based predictive control of variable speed limits. Transport. Res. Part C: Emerg. Technol. 77, 405–420.

Hegyi, A., De Schutter, B., Hellendoorn, J., 2003. MPC-based optimal coordination of variable speed limits to suppress shock waves in freeway traffic. In: Proceedings of the 2003 American Control Conference, pp. 4083–4088.

Hegyi, A., Hoogendoorn, S., Schreuder, M., Stoelhorst, H., Viti, F., 2008. SPECIALIST: A dynamic speed limit control algorithm based on shock wave theory. In: 11th International IEEE Conference on Intelligent Transportation Systems, pp. 827–832.

Jacquet, D., Jaglin, J., Koenig, D., Canudas De Wit, C., 2006. Non-local feedback ramp metering controller design. In: Proceedings of the 11th IFAC Symposium on Control in Transportation Systems, CTS 2006.

Kurzhanskiy, A.A., 2009. Set-valued estimation of freeway traffic density. IFAC Proc. Vol. 42 (15), 271–277.

Lemarchand, A., Koenig, D., Martinez, J.J., 2011. Smooth switching Hinf/PI controller for local traffic on-ramp metering, an LMI approach. In: 18th IFAC World Congress on IFAC Proceedings Volumes, vol. 44(1), pp. 13882–13887.

Lighthill, M.J., Whitham, G.B., 1955. On kinematic waves II.: A theory of traffic flow on long crowded roads. Proc. R. Soc. Lond. A: Math., Phys. Eng. Sci. 229 (1178), 317–345.

Morarescu, I.C., Canudas De Wit, C., 2011. Highway traffic model-based density estimation. In: 2011 American Control Conference - ACC 2011. San Francisco, California, United States.

Morbidi, F., Ojeda, L.L., de Wit, C.C., Bellicot, I., 2014. A new robust approach for highway traffic density estimation. In: 2014 European Control Conference (ECC), pp. 2575–2580.

Munoz, L., Sun, X., Horowitz, R., Alvarez, L., 2003. Traffic density estimation with the cell transmission model. In: Proceedings of the 2003 American Control Conference ACC: June 4–6, 2003. Denver, Colorado, USA.

Muralidharan, A., Horowitz, R., 2015. Computationally efficient model predictive control of freeway networks. Transport. Res. Part C: Emerg. Technol. 58, 532–553.

Papageorgiou, M., Kosmatopoulos, E., Papamichail, I., 2008. Effects of variable speed limits on motorway traffic flow. Transport. Res. Rec.: J. Transport. Res. Board 2047, 37–48.

Pisarski, D., de Wit, C.C., 2012. Analysis and design of equilibrium points for the cell-transmission traffic model. In: 2012 American Control Conference (ACC), pp. 5763–5768.

Richards, P.I., 1956. Shock waves on the highway. Operat. Res. 4 (1), 42–51.

Schmitt, M., Goulart, P., Georghiou, A., Lygeros, J., 2015, Flow-maximizing equilibria of the cell transmission model. In: 2015 European Control Conference (ECC), pp. 2634–2639.

Sontag, E., 1981. Nonlinear regulation: the piecewise linear approach. IEEE Trans. Autom. Control 26 (2), 346–358.

Soriguera, F., Martinez, I., Sala, M., Menendez, M., 2017. Effects of low speed limits on freeway traffic flow. Transport. Res. Part C: Emerg. Technol. 77, 257–274.

Sun, X., Munoz, L., Horowitz, R., 2003. Highway traffic state estimation using improved mixture Kalman filters for effective ramp metering control. In: Proceedings of the 42nd IEEE Conference on Decision and Control. Maui, HI, pp. 9–12.

Sun, Y., Work, D.B., 2014. A distributed local Kalman consensus filter for traffic estimation. In: 53rd IEEE Conference on Decision and Control, pp. 6484–6491.

Thai, J., Bayen, A., 2013. State estimation for polyhedral hybrid systems and applications to the Godunov scheme. In: Proceedings of the 16th International Conference on Hybrid Systems: Computation and Control. New York, NY, USA, pp. 143–152.

Thai, J., Bayen, A., 2015. State estimation for polyhedral hybrid systems and applications to the Godunov scheme for highway traffic estimation. IEEE Trans. Autom. Control 60 (2), 311–326.

Vivas, C., Siri, S., Ferrara, A., Sacone, S., Cavanna, G., Rubio, F.R., 2015. Distributed consensus-based switched observers for freeway traffic density estimation. In: 54th IEEE Conference on Decision and Control (CDC), pp. 3445–3450.